Applied Nanoscience (2021) 11:1759–1768
https://doi.org/10.1007/s13204-021-01818-3

ORIGINAL ARTICLE

Omnidirectional high reflector at 650, 850, 1300 and 1550 nm for optical fiber communication by fused silica/YBCO-superconductor Octonacci photonic crystal

Naim Ben Ali[1,2] · Haitham Alsaif[3] · Youssef Trabelsi[4,2] · Yassine Bouazzi[1,2] · Mohamed Ben Rabeh[2]

Received: 23 February 2021 / Accepted: 22 March 2021 / Published online: 10 April 2021

Abstract

The transfer matrix method (TMM) is deployed to determine the reflectance spectra of Octonacci photonic structures. First, the structures are designed using the TiO_2 and SiO_2 slabs materials. This design allows the obtainment of limited high reflectors for some optical communication wavelengths and for both TE and TM polarizations. After that, the superconductor $YBa_2Cu_3O_7$ (YBCO) and the silica slabs replace the previous materials in Octonacci structures. This modification permits to extend the omni-directional reflectance bands for both polarizations. The iteration number of the Octonacci sequence has an important effect on these bands. Later the geometric thickness of the photonic structure is optimized by changing the reference wavelength λ_0 and omnidirectional high reflectors that cover all optical communication wavelengths (650, 850, 1300 and 1550 nm) are obtained. In addition, for these wavelengths, a tiny effect of the ambient temperature is noticed. These omnidirectional high reflectors can find application in glass (GFO) and plastic (PFO) fiber optics and may be used in sensing applications.

Keywords Photonic crystal · Octonacci · Superconductor · High reflector · Fiber optic

Introduction

The discovery of electricity permits to humans the use of electronic signals to transmit information inside copper wires and as an example; we find the old-wired phone and the Internet distributed through the wired network. However, this technology was accompanied by many problems, such as the raise of temperature inside the devices due to the Joule effect, its energy consumption, and its limited transfer of data. However, the substitution of the light pulses instead of electronic pulses offers solution to all these problems. In fact light made of photons travels much faster than electrons and consumes less energy and is not accompanied by the Joule effect. In addition, light can transmit more information flow. The optical communication also known as optical telecommunication uses light (optical signal) to carry information from a start location (sender) to its destination (receiver). A transmitter (can be laser or LED sources) is used to encode the information into an optical signal and a channel (a physical transmission medium such as the fiber-optic cable) is requested to convey the optical signals along it over long distances. The capacity of channel for transmitting information is measured by its data rate in bits per second or by its bandwidth in Hz. At the destination point of the system (the end point), the optical signal is received by photodiodes and converted back into electronic signals (Ohring 2002).

The visible spectrum that our eyes can detect goes from 400 to 700 nm (from violet to red).Under the red begin the infrared spectrum. The glass fiber optics (GFO) operate along the wavelengths 850, 1300 and 1550 nm. The attenuation (due to absorption and scattering) of this fiber is much less around these wavelengths values. The absorption

✉ Naim Ben Ali
naimgi2@yahoo.fr

1 Department of Industrial Engineering, College of Engineering, University of Ha'il, Ha'il City 2440, Saudi Arabia

2 Photovoltaic and Semiconductor Materials Laboratory, University of Tunis El Manar, National Engineering School of Tunis, 1002 Tunis, Tunisia

3 Department of Electrical Engineering, College of Engineering, University of Ha'il, Ha'il City 2440, Saudi Arabia

4 College of Arts and Sciences in Muhail Asir, Physics Department, King Khalid University, Abha, Saudi Arabia

happens due to the tiny amounts of water vapor in glass; it exists in several wavelength bands called water bands. Scattering occurs when light is diffused by atoms or molecule in the glass. The lower scattering is found with longer wavelengths. There exist two families for the GFO: the multimode graded index fiber operates along the wavelengths 850 and 1300 nm; however, the single-mode fiber operates along 1310 and 1550 nm. Also for the shorter wavelengths like 650 nm of the red light and 850 nm the scientists develop plastic fiber optics (PFO) because the plastic material has lower absorption at these wavelengths (Rajiv 2002).

The photonic crystals (Brandao et al. 2015; Trabelsi 2019; Baraket et al. 2017; Chung-An et al. 2013; Srivastava 2014; Wu and Gao 2015; Ali et al. 2010) are made by alternating two or more different materials layers. This alternation can be periodic or aperiodic which makes it possible to build periodic or quasi-periodic photonic crystals such as Fibonacci, Octonacci, Thue-Morse, Cantor etc. (Brandao et al. 2015; Trabelsi 2019; Baraket et al. 2017; Chung-An et al. 2013; Srivastava 2014; Wu and Gao 2015; Ali et al. 2010). These crystals are being studied by several researchers with the aim of building omnidirectional mirrors (Pandey et al. 2017; Nayak et al. 2019; Hsueh et al. 2010; Sayed et al. 2020), sensors (Qutb et al. 2021; Zaky 2021; Amiri et al. 2019; Shaban et al. 2020; Nouman et al. 2020), filters (Aly et al. 2020; Aly and Mohamed 2019), etc.… The omnidirectional mirrors have many applications, both for reflecting surfaces, for improving the performance of LEDs, or for their properties of very high reflectivity in the optical cavities of certain lasers (e.g.: VCSEL) (Ariza-Flores et al. 2012). In addition, these mirrors find applications in high-frequency band as an antenna substrate (Zandi et al. 2007), in optoelectronics devices (Ali and Kanzari 2010; Pandey 2012; Srivastava et al. 2008) and in optical communication devices (Gahef et al. 2017). Moreover, these photonic omnidirectional mirrors are useful to construct the multi-quantum wells (MQW) for the optical regeneration by saturable absorbers (SA) applications (Takahashi 1790; Mangeney et al. 2000).

In this paper, we search to construct omnidirectional mirrors using Octonacci photonic structure filled with silica and superconductor materials. In addition, the geometric and optical properties of these mirrors are optimized. We aim that these mirrors cover the operational wavelengths of the PFO and GFO devices.

Theoretical model

Octonacci sequence

The photonic crystal layers are arranged according to the Octonacci (Brandao et al. 2015) sequence $S_n = S_{n-1} \times S_{n-2} \times S_{n-1}$, where n is the iteration number, $S_1 = H$ and $S_2 = L$. Here H and L represent the layer of high and low refractive index value respectively. Figure 1 illustrates an example of the geometric structure of the 4th Octonacci iteration. The used materials during this theoretical investigation are SiO_2, TiO_2 and yttrium barium copper oxide (YBCO). The Gorter–Casimir two-fluid model is used to describe the optical response of the YBCO superconductor. The external magnetic field is supposed to be null (Trabelsi 2019; Baraket et al. 2017; Chung-An et al. 2013; Srivastava 2014; Wu and Gao 2015). The refractive index of the YBCO superconductor depends on the ambient temperature T and the wave-frequency ω (Trabelsi 2019; Baraket et al. 2017; Chung-An et al. 2013; Srivastava 2014; Wu and Gao 2015): $n_s = \sqrt{\varepsilon_s} = \sqrt{1 - \frac{1}{\omega^2 \mu_0 \varepsilon_0 \lambda_L^2(T)}}$. Here $\lambda_L(T) = \frac{\lambda_p}{\sqrt{1-G(T)}}$ represents the temperature-dependent penetration depth, $\mu_0$andε_0 symbolize, respectively, the permeability and the permittivity of free space (Trabelsi 2019; Baraket et al. 2017; Chung-An et al. 2013; Srivastava 2014; Wu and Gao 2015). In the last formula and at $T = 0$ K, the London penetration depth is $\lambda_p = 140$ nm. $G(T) = \left(\frac{T}{T_c}\right)^4$ is the Groter–Casimir expression. In addition, T represents the ambient temperature and $T_c = 92$K is the superconducting critical temperature (Trabelsi 2019; Baraket et al. 2017; Chung-An et al. 2013; Srivastava 2014; Wu and Gao 2015).

Transfer matrix method (TMM)

To extract the reflectance spectra, the transfer-matrix method (TMM) is employed. This method is introduced by Yeh and Yariv (1984) and Ali et al. (2020) and allows to determine the optical properties (reflectance, transmittance, absorption, electromagnetic field, etc.) of the multilayered structures. When juxtaposing successive layers, the amplitudes of the electric fields of incident wave

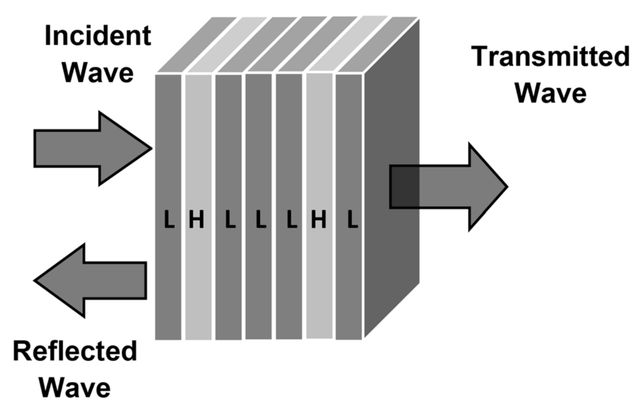

Fig. 1 Schematic representation showing the geometric structure of 4th Octonacci iteration

E_0^+, reflected wave E_0^- and transmitted wave E_{m+1}^+ after m layers can be correlated via the following formula (Yeh and Yariv 1984; Ali et al. 2020):

$$\begin{pmatrix} E_0^+ \\ E_0^- \end{pmatrix} = \frac{C_1 C_2 C_3 \ldots C_{m+1}}{t_1 t_2 t_3 \ldots t_{m+1}} \begin{pmatrix} E_{m+1}^+ \\ E_{m+1}^- \end{pmatrix}, \quad (1)$$

where the C_j(propagation matrix) for the jth layer is:

$$C_j = \begin{pmatrix} \exp\left(i\varphi_{j-1}\right) & r_j \exp\left(-i\varphi_{j-1}\right) \\ r_j \exp\left(i\varphi_{j-1}\right) & \exp\left(-i\varphi_{j-1}\right) \end{pmatrix}, \quad (2)$$

φ_{j-1} indicates the phase shift of the wave between $(j-1)$th and jth boundaries and can be determined as:

$$\varphi_0 = 0, \quad (3)$$

$$\varphi_{j-1} = \frac{2\pi}{\lambda} \hat{n}_{j-1} d_{j-1} \cos\theta_{j-1}, \quad (4)$$

where $\hat{n}_j$ and θ_j are the complex refractive index and the complex refractive-wave angle, respectively.

For parallel P-polarization (TM mode), the Fresnel coefficients t_j and r_j are (Yeh and Yariv 1984; Ali et al. 2020):

$$r_{jp} = \frac{\hat{n}_{j-1}\cos\theta_j - \hat{n}_j \cos\theta_{j-1}}{\hat{n}_{j-1}\cos\theta_j + \hat{n}_j \cos\theta_{j-1}}, \quad (5)$$

$$t_{jp} = \frac{2\hat{n}_{j-1}\cos\theta_{j-1}}{\hat{n}_{j-1}\cos\theta_j + \hat{n}_j \cos\theta_{j-1}}. \quad (6)$$

Moreover, for perpendicular S-polarization (TE mode) (Yeh and Yariv 1984; Ali et al. 2020):

$$r_{js} = \frac{\hat{n}_{j-1}\cos\theta_{j-1} - \hat{n}_j \cos\theta_j}{\hat{n}_{j-1}\cos\theta_{j-1} + \hat{n}_j \cos\theta_j}, \quad (7)$$

$$t_{js} = 2\frac{\hat{n}_{j-1}\cos\theta_{j-1}}{\hat{n}_{j-1}\cos\theta_{j-1} + \hat{n}_j \cos\theta_j}. \quad (8)$$

For both polarization modes S and P the transmittance energy are:

$$T_S = \mathrm{Re}\left(\frac{\hat{n}_{m+1}\cos\theta_{m+1}}{\hat{n}_0 \cos\theta_0}\right)\left|t_S\right|^2, \quad (9)$$

$$T_P = \mathrm{Re}\left(\frac{\hat{n}_{m+1}\cos\theta_{m+1}}{\hat{n}_0 \cos\theta_0}\right)\left|t_P\right|^2, \quad (10)$$

Re indicates the real part (Yeh and Yariv 1984; Ali et al. 2020).

Results and discussions

Materials effect

We begin this work by studying the material effect on the width of the photonic band gap (PBG). First, we choose SiO_2 and TiO_2 as two materials of the Octonacci layers with refractive indices 1.45 and 2.3, respectively. We choose these two materials because of their availability, its costs are cheaper compared with other types of semiconductor materials and it is easy to fabricate photonic crystals with them. The optical thickness $n \times d$ of layers is chosen to satisfy the Bragg's condition: $n \times d = \frac{\lambda_0}{4}$, where λ_0 is the reference wavelength (Ali et al. 2020). The iteration of the Octonacci multilayered structure is fixed at 5, so the structure's number of layers P is equal to 17. The λ_0 is chosen to be equal to 1.5 µm; therefore, the structure thickness ds is equal to 3.92 µm. Figure 2 displays the 3D reflectance spectra as function of wavelength (µm) and incident angle (rad) for TE and TM wave-polarization. In Fig. 2 the PBGs areas are showed with yellow color and they are separated by several Bragg peaks in blue color for different wavelengths and incident angle.

Table 1 summarizes the intervals of wave-incident-angle for which the optical communication wavelengths are totally reflected. From Fig. 2 and Table 1, we can conclude that the wavelengths of the single-mode fiber (1300 and 1550 nm) are often transmitted through the photonic structure for TM-mode, and reflected for some incident angle when the wave is TE-polarized. The wavelengths 650 and 850 nm of the PFO and the multimode graded index fiber are often propagated through the Octonacci structure.

To expand the PBGs to cover all optical communication wavelengths, we try now to change the layers of TiO_2 materials with the superconductor yttrium barium copper oxide $YBa_2Cu_3O_7$ (YBCO). This superconductor is a high-temperature superconductors and let know that a superconductor with Tc more than 30 K, is generally considered to be the high-temperature superconductor (HTS) material otherwise the superconductor is considered to be the low-temperature superconductor (LTS) material. In addition, this superconductor has stimulated interest in manufacturing economic because the efficient cost of refrigeration to superconducting temperatures (often requiring cryogens such liquid nitrogen or liquid helium) of the HTS are less than that needed by the LTS material. Furthermore, the YBCO superconductor has been most successfully used in the form of epitaxial thin films or as single crystals.

Figure 3 illustrates the reflectance spectra for TE and TM wave-polarization. The reference wavelength and the number of layers are kept fixed $\lambda_0 = 1.5$ µm, $P = 17$. The

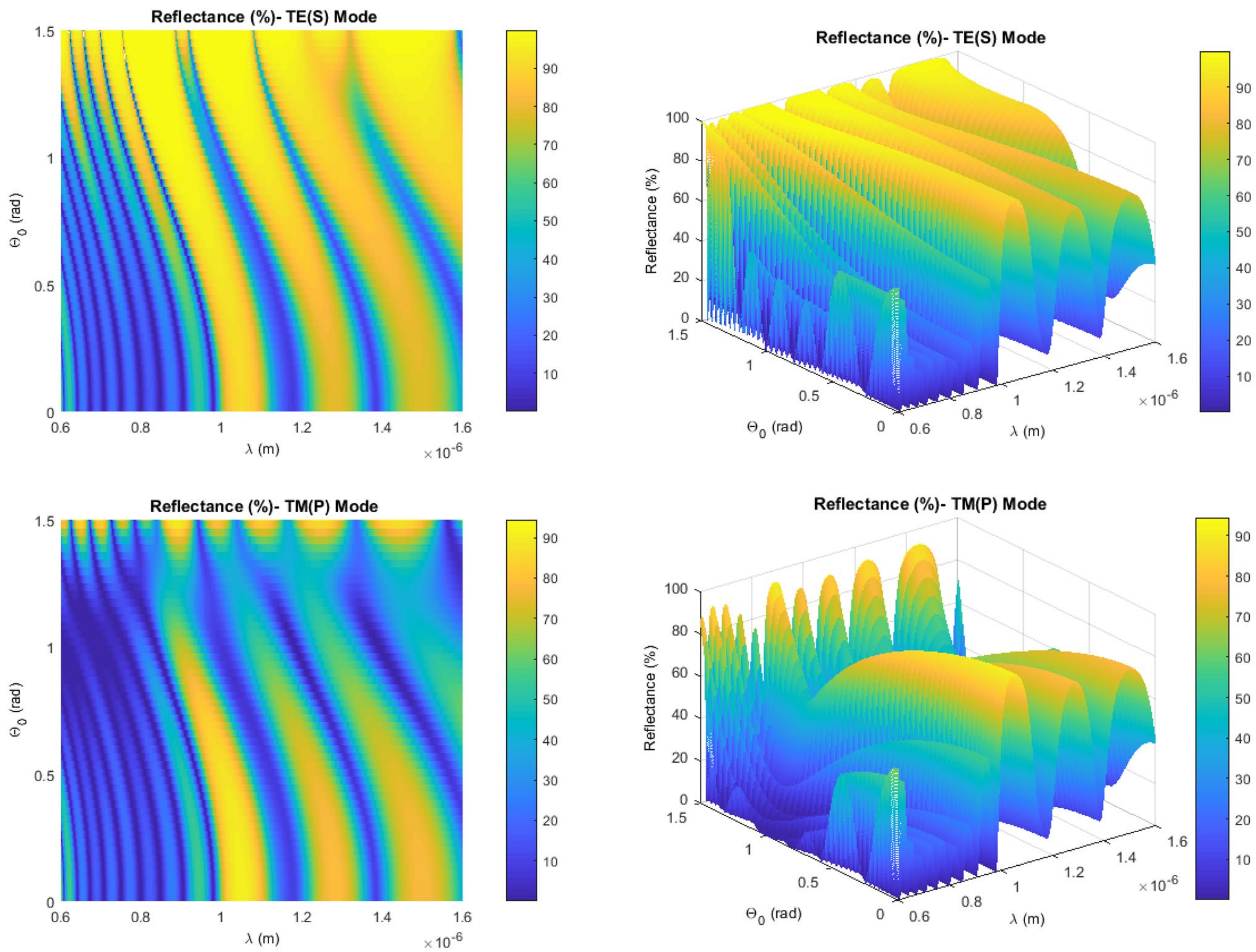

Fig. 2 3D Reflectance spectra of 1D Octonacci multilayered stack (with TiO_2 and SiO_2 materials) as a function of wavelength (µm) and incident angle (rad) for TE- and TM-polarization modes: $\lambda_0 = 1.5$ µm, $P = 17$ and ds = 3.92 µm

Table 1 Intervals of incident angle for which the optical communication wavelengths are totally reflected

Optical communication wavelengths (nm)	Totally reflectance area	
	TE-mode (rad)	TM-mode
650	$\theta_0 \geq 1.37$	$\theta_0 \geq 1.44$rad
850	$\theta_0 \geq 0.98$	–
1300	$\theta_0 \leq 0.34$ and $\theta_0 \geq 0.79$	$\theta_0 \leq 0.27$rad
1550	$\theta_0 \geq 0.76$	–

The structure is Octonacci with TiO_2 and SiO_2 materials ($\lambda_0 = 1.5$ µm, $P = 17$ and ds = 3.92 µm)

ambient temperature is set at 25 °C. The geometric thickness of the new Octonacci structure becomes ds = 3.2 µm. In addition, Table 2 shows the intervals of wave-incident-angle for which the optical communication wavelengths are totally reflected. It is clear from Fig. 3 and Table 2 that the wavelengths of the single-mode fiber (1300 and 1550 nm) are totally reflected, but the wavelengths 650 and 850 nm of the PFO and the multimode graded index fiber are often propagated through the Octonacci structure. Therefore, we can conclude that the replacement of the TiO_2 layers with the YBCO layers permits the expansion of the main PBG, this physical phenomenon is due to the increase of the refractive index contrast between the materials that compose the photonic structure.

In the next part, and by changing the iteration number of Octonacci sequence, we will try to enlarge the PBG to cover these two last wavelengths.

Iteration effect

In this part, the iteration number of the Octonacci sequence is changed in order to enlarge the omnidirectional PBGs. The increase of the iteration number permits to change the number of layers and the thickness of the whole structure which permits to change the PBGs width.

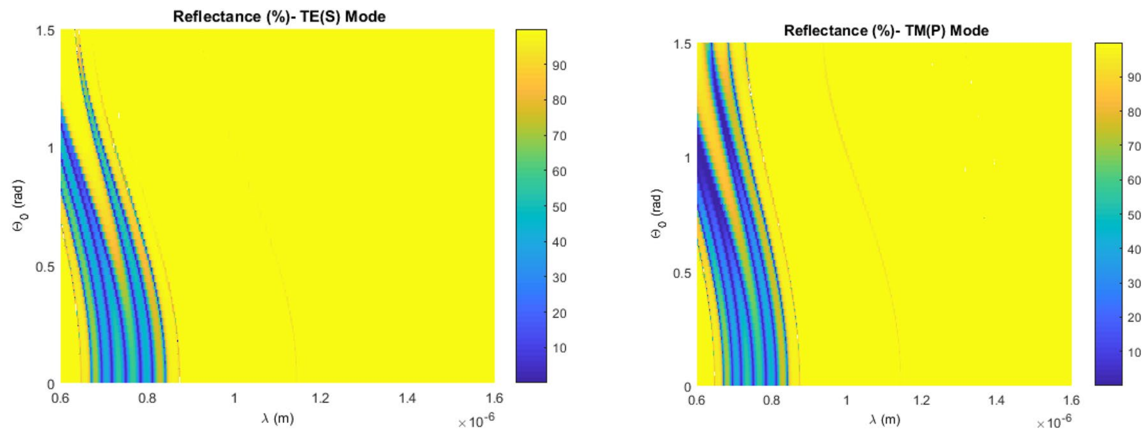

Fig. 3 Reflectance spectra of 1D Octonacci multilayered stack (with YBCO and SiO2 materials) as a function of wavelength (μm) and incident angle (rad) for TE- and TM-polarization modes: $\lambda_0 = 1.5$ μm, $P = 17$ and ds = 3.2 μm

Table 2 Intervals of incident angle for which the optical communication wavelengths are totally reflected

Optical communication wavelengths (nm)	Totally reflectance area	
	TE-mode (rad)	TM-mode (rad)
650	$\theta_0 \le 0.33$, $0.92 \le \theta_0 \le 1.19$ and $\theta_0 \ge 1.37$	$\theta_0 \le 0.28$, $0.98 \le \theta_0 \le 1$ and $\theta_0 \ge 1.47$
850	$\theta_0 \le 0.37$ and $\theta_0 \ge 0.43$	$\theta_0 \le 0.4$ and $\theta_0 \ge 0.46$
1300	$0 \le \theta_0 \le 1.$	$0 \le \theta_0 \le 1.5$
1550	$0 \le \theta_0 \le 1.5$	$0 \le \theta_0 \le 1.5$

The structure is Octonacci with YBCO and SiO_2 materials ($\lambda_0 = 1.5$ μm, $P = 17$ and ds = 3.2 μm

Therefore, in this part, we will change the number of iteration and keep the minimum one that permits to cover all-optical fiber wavelengths. The reference wavelength λ_0 is still fixed at 1.5 μm and the ambient temperature is 25 °C. Figure 4 shows the reflectance spectra for both polarization modes. In Fig. 4a the iteration number is changed to 6, so the number of layers P becomes 41 and the structure thickness is ds = 7.73 μm. In addition, Fig. 4b shows the reflectance spectra when the iteration number is equal to 7, therefore, the number of layers P becomes 99 and the structure thickness is ds = 18.67 μm. When changing the Octonacci iteration number and by comparing Fig. 4a and b with Fig. 3, we can conclude that the wavelengths 1300 and 1550 nm are still omnidirectional reflected. However, we note a slight improvement in the reflection range of the wavelengths 650 and 850 nm. Therefore, in the next parts, we will keep the iteration number fixed at 5 and we will study the effect of the layer thickness on the reflection of the optical communication wavelengths.

Layers thickness effect

The layers thickness is monitored by changing the reference wavelength λ_0. Figure 5 shows the reflectance spectra depends on λ_0 for both polarization modes. The iteration number and the ambient temperature are set at 5 and 25 °C respectively. The geometric thickness of the structure is ds = 2.13 μm. Figure 3 and Fig. 5a show the reflection spectra for the same iteration number $P = 5$. In Fig. 5a and for TE and TM modes there are only two brown lines in which the reflectance ratio is more than 95%. Therefore, we notice here that when reducing λ_0 from 1.5 to 1 μm all the optical communication wavelengths (650, 850, 1300 and 1550 nm) are reflected regardless of θ_0 value. In Fig. 5b the λ_0 becomes equal to 0.5 μm, so thickness of the structure is ds = 1.07 μm. Here for TE mode, the wavelength 650 nm is reflected only when $\theta_0 \le 0.79$rad and $\theta_0 \ge 0.85$rad and the rest of the optical communication wavelengths are fully omnidirectional reflected. In addition, in Fig. 5b and for TM mode the wavelength 650 nm is reflected only when $\theta_0 \le 0.73$rad and $\theta_0 \ge 0.82$rad. The wavelength 1550 nm is reflected for $\theta_0 \le 1.34$rad and the rest of the optical communication wavelengths are totally reflected. In Fig. 5c the reference wavelength λ_0 is changed to 0.25 μm, therefore, the geometric thickness of the structure becomes ds = 0.53 μm. For TE mode, the wavelengths 850 and 1550 nm are transmitted for some intervals of the incident angle θ_0 and for TM mode all the optical communication wavelengths are not omnidirectional reflected. So at the end of this part we can conclude that, the best value of the reference wavelength λ_0 for which all the optical communication wavelengths are omnidirectional reflected is 1 μm. Physically this phenomenon is due to the convergence between the optical layer thickness $\left(\frac{\lambda_0}{4 \times n}\right)$ and the central wavelength spectrum value. Indeed, our

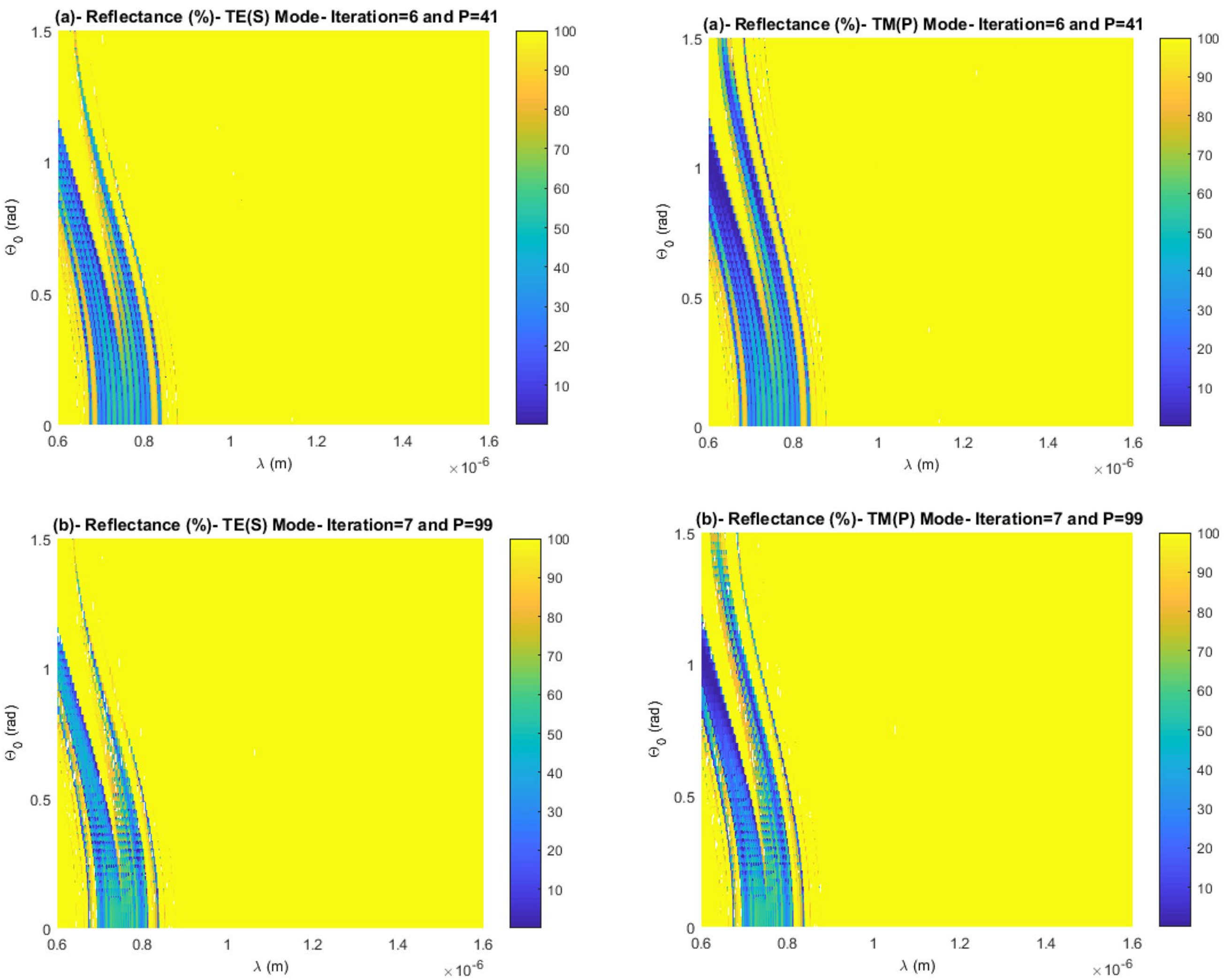

Fig. 4 Reflectance spectra of 1D Octonacci multilayered stack (with YBCO and SiO_2 materials $\lambda_0 = 1.5$ µm) as a function of wavelength (µm) and incident angle (rad) for TE- and TM-polarization modes: **a** iteration = 6, $P = 41$ and **b** iteration = 7, $P = 99$

spectrum is [0.6–1.6 µm], so the coincidence of the value of λ_0 with the center of this interval (approximately 1 µm) allows us to have a large PBG centered at this value and cover the majority of optical fiber wavelengths. In addition, when changing the iteration number from 7 to 5 and the reference wavelength λ_0 to 1 µm, the geometric thickness of the structure is optimized to be ds = 2.13 µm.

Ambient temperature effect

For this part, we keep the iteration number P and the reference wavelength λ_0 fixed at 5 and 1 µm, respectively, and we try now to study the dependence between the temperature and the reflectance spectra of the optical communication wavelengths. Figure 6 displays the variation of the reflectance spectra with the temperature T and for both polarization modes. From Fig. 6, it turns out that the weather temperature has little effect on the reflectance spectra of the optical communication wavelengths. When $T = 0$ °C and for the TM mode (see Fig. 6a) only the wavelength 650 nm has a reflectance of 65% when $0.85 \leq \theta_0 \leq 0.95\text{rad}$, and the other wavelengths have a reflectance of more than 85%. After that when increasing the temperature to be more than 20 °C all the optical communication wavelengths become high reflected regardless of θ_0 value. These structures open the way to be used as optical devices in the optical industry. Then we can conclude that the structure can keep their reflectance performance whatever the temperature degree of the environment. In fact, the refractive index of the YBCO materials depends on temperature and increases with it. Indeed, when the temperature is 0 °C only the wavelength 650 nm cannot be totally reflected. After that, and with the increase of temperature the refractive index of YBCO

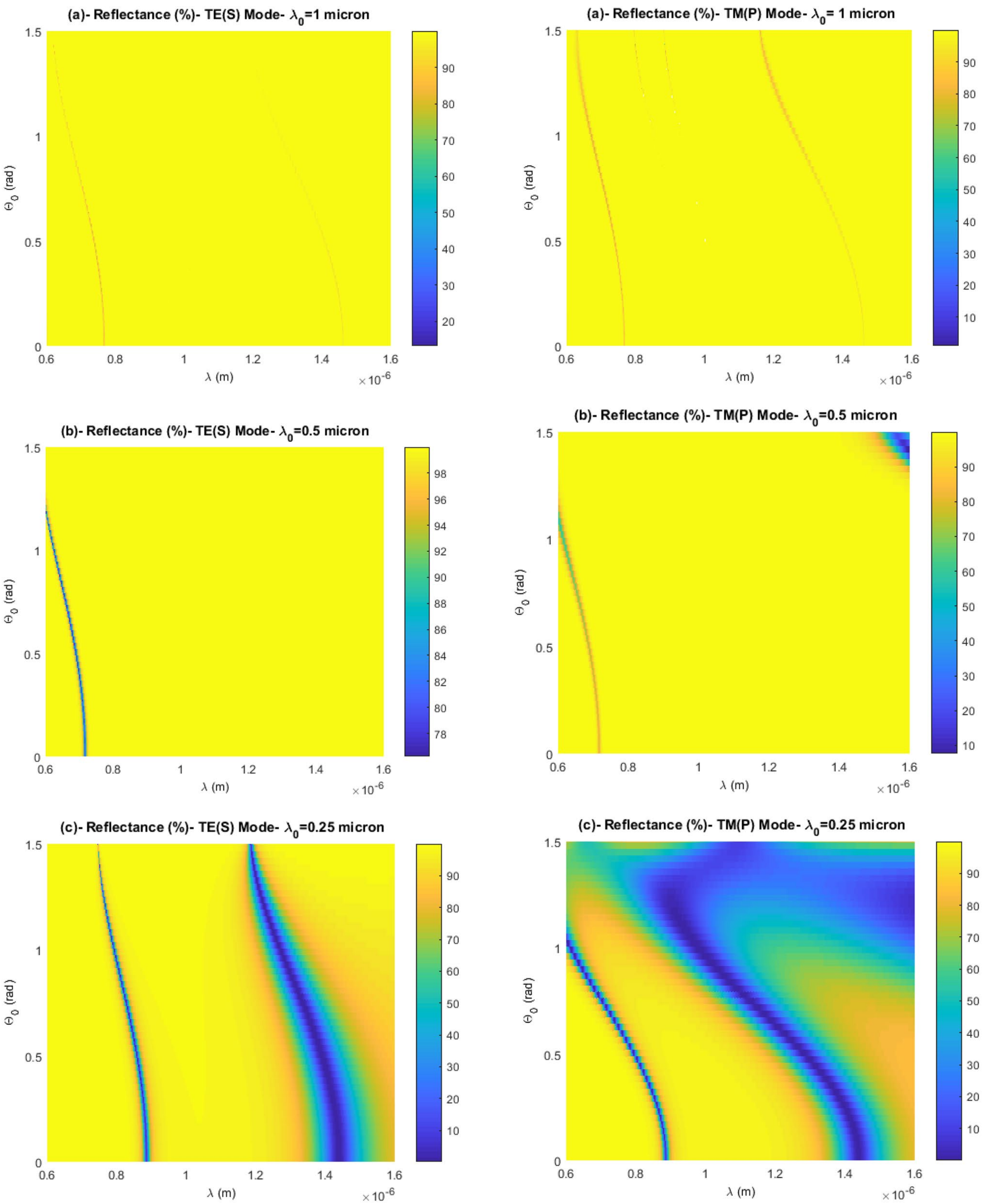

Fig. 5 Reflectance spectra of 1D Octonacci multilayered stack (with YBCO and SiO_2 materials $\lambda_0 = 1.5$ μm) as a function of wavelength (μm) and incident angle (rad) for TE- and TM-polarization modes: **a** $\lambda_0 = 1$ μm, **b** $\lambda_0 = 0.5$ μm and **c** $\lambda_0 = 0.25$ μm

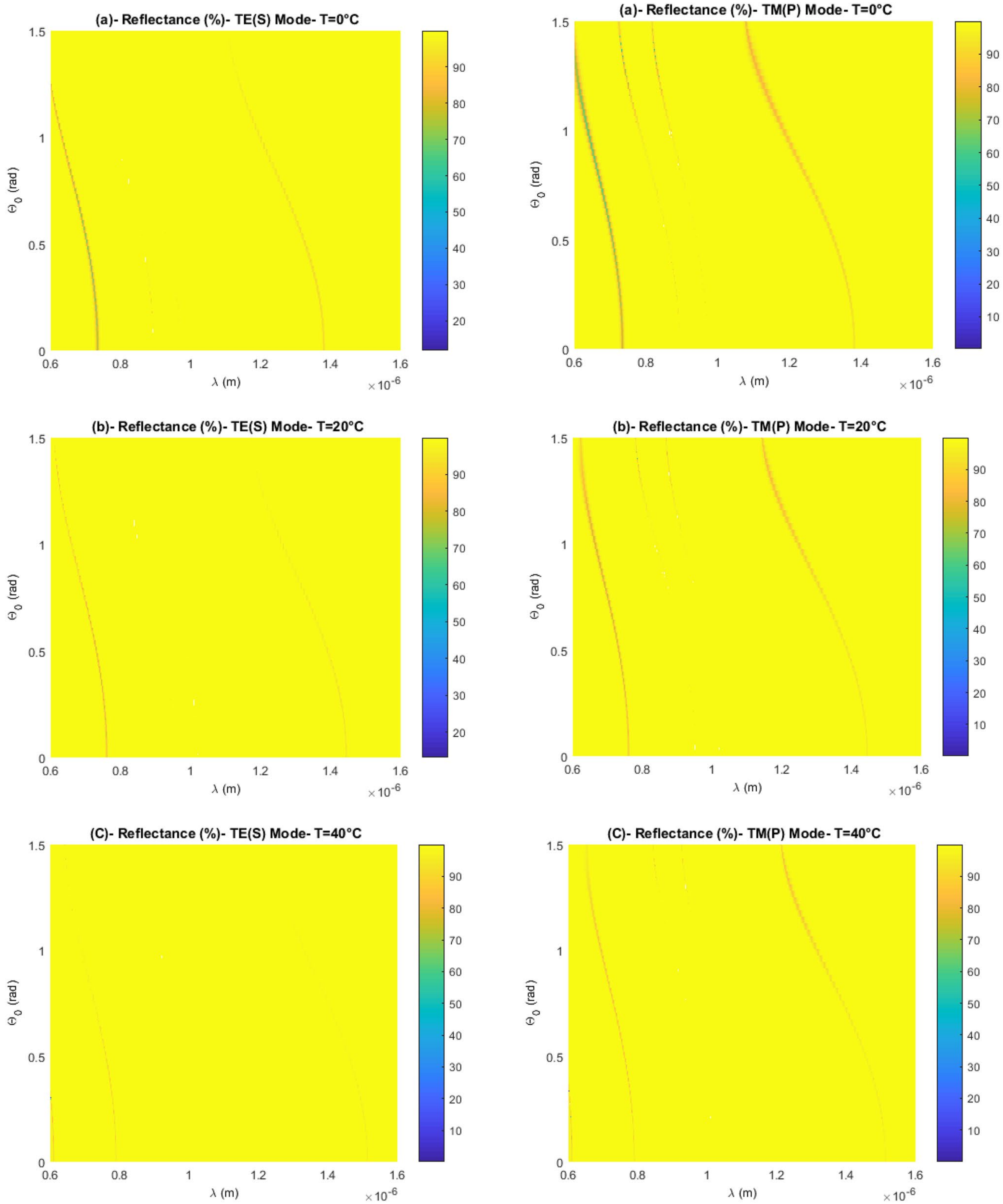

Fig. 6 Reflectance spectra of 1D Octonacci multilayered stack (with YBCO and SiO2 materials $\lambda_0 = 1$ µm) as a function of wavelength (µm) and incident angle (rad) for TE- and TM-polarization modes: **a** $T = 0$ °C, **b** $T = 20$ °C, **c** $T = 40$ °C, **d** $T = 60$ °C

layers increases which permits the enlargement of the main PBG to cover all-optical fiber wavelengths.

Comparison with some previous works

The published paper of Pandey et al. (2017), studied plasma photonic crystal (PPC) which consists of alternate layers of thin micro-plasma with dielectric material in one-dimensional periodic structure (containing SiO_2 and Air layers). By introducing the plasma defect inside the periodic structure the band gap is slightly widened and containing two transmission peaks in symmetry (Pandey et al. 2017). In addition, Nayak et al. (2019) studied the near- and mid-infrared PBGs using periodic photonic structure that was composed of superconductor and semiconductor-metamaterial. They found and optimized two PBGs by manipulating the thickness of the semiconductor layers, the fill factor of the semiconductor-metamaterial and the wave-incidence. The researcher here (Nayak et al. 2019) found that for the TM polarization, the PBGs disappeared at the incident angles of approximately 1.05 rad. In addition The PBGs does not cover all the near- and mid-infrared spectrum. Furthermore, Hsueh et al. (2010), studied one-dimensional periodic structure in multiple frequency ranges and for both polarization. They found one maximum range of the omnidirectional gap in each region, which is divided by the half-wave lines. The paper of Ariza-Flores et al. (2012), shows a comparison between theoretical and experimental study of the omnidirectional photonic bandgap for dielectric mirrors based on porous silicon. Here (Ariza-Flores et al. 2012), the main PBG covers only the spectral range [1100–1195 nm]. The paper of Ali and Kanzari (2010), studied a modified hybrid Fibonacci/Cantor structure showed a mirror covering only the optical telecommunication wavelengths centered at 850 nm, 1300 nm and 1550 and for the incident angles situated outside of the range [0.91–1.43 rad]. In addition, Gahef et al. (2017) presents an omnidirectional mirror covering only the optical fibers wavelengths 1300 and 1550 nm using a deformed Bragg reflector. Finally, by comparing these previous published works with our own, we can notice the importance of using Octonacci structure instead of periodic structures as well the importance of using the YBCO superconductor instead of ordinary materials if we seek to enlarge the PBG to cover all the optical communication wavelengths (650, 850, 1300 and 1550 nm).

Conclusion

At the end of this paper, we can conclude that using the semiconductor YBCO and silica slabs in Octonacci photonic crystal instead of the TiO_2 and SiO_2 slabs permits to construct omnidirectional high reflectors for the optical communication wavelengths (650, 850, 1300 and 1550 nm). By changing the reference wavelength λ_0 to be equal to 1 µm, the geometric thickness of the photonic structure is optimized to be ds = 2.13 µm. In addition, the reflectance ratio of the optical communication wavelengths is significantly improved. In last part of this paper, the weather temperature effect on the reflectance spectra has been studied and a small effect on the reflectance ratio of these wavelengths is noticed. Whereas the most optical communication wavelengths were reflected with large rates that exceeded 85%. Only the 650 nm wavelength was 65% reflected when the wave is TM-polarized, the wave incident angle is $0.85 \leq \theta_0 \leq 0.95$rad and the weather temperature is 0 °C. As a perspective of this work, we can conclude that these structures can be realized experimentally and compared with the theoretical results found here.

Acknowledgements "This research has been funded by Scientific Research Deanship at University of Ha'il—Saudi Arabia through project number RG-20 021".

Declarations

Conflict of interest The authors declare that they have no known competing financial interests or personal relationships that could have appeared to influence the work reported in this paper.

References

Ali NB, Kanzari M (2010) Designing of omni-directional high reflectors by using one-dimensional modified hybrid Fibonacci/Cantor band-gap structures at optical telecommunication wavelength band. J Mod Opt 57(4):287–294. https://doi.org/10.1080/09500340903545289

Ali NB, Zaghdoudi J, Kanzari M, Kuszelewicz R (2010) The slowing of light in one-dimensional hybrid periodic and non-periodic photonic crystals. J Opt 12:045402

Ali NB, Dhasarathan V, Alsaif H, Trabelsi Y, Nguyen TK, Bouazzi Y, Kanzari M (2020) Design of output-graded narrow polychromatic filter by using photonic quasicrystals. Phys B 582:411918. https://doi.org/10.1016/j.physb.2019.411918

Aly AH, Sayed FA, Elsayed HA (2020) Defect mode tunability based on the electro-optical characteristics of the one-dimensional graphene photonic crystals. Appl Opt 59(16):4796–4805. https://doi.org/10.1364/AO.393689

Aly AH, Mohamed D (2019) The optical properties of metamaterial-superconductor photonic band gap with/without defect layer. J Supercond Nov Magn 32:1897–1902. https://doi.org/10.1007/s10948-018-4922-2

Amiri IS, Paul BK, Ahmed K, Aly AH, Zakaria R, Yupapin P, Vigneswaran D (2019) Tri-core photonic crystal fiber based refractive index dual sensor for salinity and temperature detection. Microw Opt Technol Lett 61(3):847–852. https://doi.org/10.1002/mop.31612

Ariza-Flores AD, Gaggero-Sager LM, Agarwal V (2012) Study of the omnidirectional photonic bandgap for dielectric mirrors based on porous silicon: efect of optical and physical thickness. Nanoscale Res Lett 7(391):1–6. https://doi.org/10.1186/1556-276X-7-391

Baraket Z, Zaghdoudi J, Kanzari M (2017) Investigation of the 1D symmetrical linear graded superconductor dielectric photonic crystals and its potential applications as an optimized low temperature sensors. Opt Mater 64:147–151

Brandao ER, Costa CH, Vasconcelos MS, Anselmo DHAL, Mello VD (2015) Octonacci photonic quasicrystals. Optical Society of America

Gahef T, Bouazzi Y, Kanzari M (2017) Omnidirectional mirror at 1.3 and 1.55 μm for optical fiber communication by specific deformation of Bragg reflector. Opt Quant Electron 49:95. https://doi.org/10.1007/s11082-017-0921-y

Hsueh WJ, Wun SJ, Yu TH (2010) Characterization of omnidirectional bandgaps in multiple frequency ranges of one-dimensional photonic crystals. JOSA B 27(5):1092–1098

Hu C-A, Liu J-W, Wu C-J, Yang Y-J, Yang S-L (2013) Effects of superconducting film on the defect mode in dielectric photonic crystal heterostructure. Solid State Commun 157:54–57

Mangeney J, Aubin G, Oudar JL, Harmand JC, Patriarche G et al (2000) All-optical discrimination at 1.5 μm using an ultrafast saturable absorber vertical cavity device. Electron Lett 36:1486. https://doi.org/10.1049/el:20001056

Nayak C, Aghajamali A, Saha A, Das N (2019) Near- and mid-infrared bandgaps in a 1D photonic crystal containing superconductor and semiconductor—metamaterial. Int J Mod Phys B 33(20):1950219. https://doi.org/10.1142/S0217979219502199

Nouman WM, El-Ghany SESA, Sallam SM et al (2020) Biophotonic sensor for rapid detection of brain lesions using 1D photonic crystal. Opt Quant Electron 52:287. https://doi.org/10.1007/s11082-020-02409-2

Ohring M (2002) Materials Science of thin films, 2nd edition, chapter 8, deposition and structure. Academic Press, pp 417–494. https://doi.org/10.1016/B978-012524975-1/50011-2

Pandey JP (2017) Omnidirectional high reflectors using 1-D photonic crystals. Int J Phys Sci 12(12):137–145. https://doi.org/10.5897/IJPS2017.4629

Pandey GN, Shukla AK, Thapa KB, Pandey JP (2017) Enhanced of photonic bandgaps in one-dimensional plasma photonic crystal with defect. In: Bhattacharya I, Chakrabarti S, Reehal H, Lakshminarayanan V (eds) Advances in optical science and engineering: proceedings in physics, vol 194. Springer, Cham. https://doi.org/10.1007/978-981-10-3908-9_26

Qutb SR, Aly AH, Sabra W (2021) Salinity and temperature detection for seawater based on a 1D-defective photonic crystal material. Int J Mod Phys B 35(1):2150012. https://doi.org/10.1142/S0217979221500120

Rajiv R (2002) Optical fiber communication: from transmission to networking. IEEE Commun Mag 40:138–147. https://doi.org/10.1109/MCOM.2002.1006983

Sayed FA, Elsayed HA, Aly AH (2020) Optical properties of photonic crystals based on graphene nanocomposite within visible and IR wavelengths. Opt Quantum Electron. https://doi.org/10.1007/s11082-020-02578-0

Shaban SM, Mehaney A, Aly AH (2020) Determination of 1-propanol, ethanol, and methanol concentrations in water based on a one-dimensional phoxonic crystal sensor. Appl Opt 59(13):3878–3885. https://doi.org/10.1364/AO.388763

Srivastava SK (2014) Study of defect modes in 1d photonic crystal structure containing high and low Tc superconductor as a defect layer. J Supercond Nov Magn 27:101–114

Srivastava R, Thapa KB, Pati S, Ojha SP (2008) Omni-direction reflection in one dimensional photonic crystal. Prog Electromagn Res B 7:133–143

Takahashi R et al (1994) Ultrafast 1.55-μm photoresponses in low-temperature-grown InGaAs/InAlAs quantum wells. Appl Phys Lett 65:1790. https://doi.org/10.1063/1.112870

Trabelsi Y, Ali NB, Kanzari M (2019) Tunable narrowband optical filters using superconductor/dielectric generalized Thue-Morse photonic crystals. Microelectron Eng 213:41–46. https://doi.org/10.1016/j.mee.2019.04.016

Wu J-j, Gao J-x (2015) Low temperature sensor based on one-dimensional photonic crystals with a dielectric-superconducting pair defect. Optik 126:5368–5371

Yeh P, Yariv A (1984) Optical waves in crystals. Wiley, New York

Zaky ZA, Aly AH (2021) Modeling of a biosensor using Tamm resonance excited by grapheme. Appl Opt 60(5):1411–1419. https://doi.org/10.1364/AO.412896

Zandi O, Atlasbaf Z, Forooraghi K (2007) Flat multylayer dielectric reflector antennas. Progress Electromagnet Res 72:1–19. https://doi.org/10.2528/PIER07022604